Available online at www.sciencedirect.com
SCIENCE DIRECT®
Journal of Colloid and Interface Science 276 (2004) 24–38
JOURNAL OF Colloid and Interface Science
www.elsevier.com/locate/jcis

Theoretical and experimental study of the interaction of O_2 and H_2O with metallic zinc—discussion of the initial step of oxide formation

G.A. Alimenti,[a] M.E. Gschaider,[a] J.C. Bazán,[a,b] and M.L. Ferreira [c,*]

[a] *UNS, Av. Alem 1253, 8000 Bahía Blanca, Argentina*
[b] *Comisión de Investigaciones Científicas de la Prov. de Buenos Aires, Buenos Aires, Argentina*
[c] *PLAPIQUI-UNS-CONICET, Camino La Carrindanga Km 7, CC 717, 8000 Bahía Blanca, Argentina*

Received 17 November 2003; accepted 18 March 2004

Available online 4 May 2004

Abstract

The steps of Zn corrosion and ZnO formation using dry O_2 or O_2/water atmosphere were investigated in situ using an experimental and theoretical approach. The adsorption equilibrium and kinetics of O_2/H_2O on Zn have been measured at different temperatures and relative humidities using a Cahn 1000 vacuum recording electrobalance. The amounts adsorbed on Zn are different in the presence or absence of O_2. SEM–EDAX, XPS, and XRD studies have been performed at the surface for different times of reaction. A theoretical study using the extended Hückel method has been done for the adsorption/reaction of H_2O/O_2 on Zn and on ZnO. A coherent explanation is presented for the initial steps of ZnO formation on Zn, for the steady state found for the ZnO growth, and for the experimental findings of the methods cited above.

Keywords: ZnO formation; Gas phase; Spontaneous corrosion

1. Introduction

Although the reaction of water with Zn to give hydrated zinc oxide is well known in the corrosion of Zn in contact with humid atmospheres, few systematic studies have dealt with the influence of water vapor pressure or relative humidity on this process of ZnO formation [1]. Several studies about ZnO structures using modern analysis techniques such as LEED and ab initio HF and LDA methods have been published [2–4]. The unrelaxed bulk Zn and O-terminated surfaces of ZnO have been compared by Overbury [5]. The process by which ZnO is formed at the Zn surface is not precisely known and the majority of the published papers about this topic are focused on the electrochemical behavior of Zn/ZnO in aqueous solution.

Zn reacts with O_2 and H_2O and has energy densities similar to common fuels. The energy density of Zn in the reaction with O_2 is 9677 Wh/kg, compared with 9741 Wh/kg for decane (comparable to gasoline). The reactive metals may be used only because of the formation of reaction product layers (passive films) on the surface. These layers protect the metal from further corrosion. It was not until the development of electron microscopy and in situ techniques such as ellipsometry and STM or AFM that researchers were able to construct physical/morphological models. The general picture is that the passive film forms a bilayer structure comprising a defective oxide layer (the primary passive film) from the metal and an outer layer via hydrolysis of cation ejected from the inner layer [6]. But this layer is complete when an aqueous medium is surrounding the metal. When the interphase is gaseous and no liquid is present this outer layer is incomplete. Steady states in oxide thickness have been observed and demonstrated in the passive films' layer thickness for Ni, Zn, and W [7,8].

Metals with low oxidation states in the barrier layer, such as Zn, form cations of the interstitial conducting *n*-type [8]. Irreversible water dissociation takes place on metal and semiconductor surfaces producing H_2, such as Zn, whereas reversible adsorption occurs on oxides such as ZnO. From different models considered, only the point defect model (PDM) in its modified form accounts for the observations summarized for the Zn/ZnO interphase. The Verwey, Cabrera, and Mott and Sato and Cohen models do not predict steady states and hence these models must be discarded [7,8]. The basis of PDM is that the barrier layer is a highly

* Corresponding author. Fax: +54-291-4861600.
E-mail address: mlferreira@plapiqui.edu.ar (M.L. Ferreira).

0021-9797/$ – see front matter
doi:10.1016/j.jcis.2004.03.042

defective defect semiconductor in which vacancies act as electronic dopants. Fluxes of cation and anion vacancies are opposite. Using this model the barrier layer of Zn was demonstrated to be an interstitial cation conductor. A complete treatment of the kinetics of growth of bilayer oxide/hydroxide structures has yet to be reported [9].

Passivity breakdown occurs as a result of cation vacancy condensation at the metal/bilayer interfaces at sites characterized by a fast cation-vacancy flux. Two processes have been postulated as being responsible for passivity breakdown. They are Schottky pair generation and cation extraction. Therefore a pit begins to grow when passivity breakdown takes place. Cation vacancy diffusivities and thickness of the barrier layer are especially important in understanding the mechanism of pit creation [6].

The open literature presents few experimental and theoretical reports on the adsorption from the gas phase of $O_2 + H_2O$ on metal surfaces. Although some interesting data on metal characterization have been published [10], there are no reports on theoretical analysis of the first steps of oxide growth on Zn by reaction with O_2/H_2O or even clear mechanisms for how this growth takes place. Recent works on ZnO thin film preparation using chemical vapor deposition (CVD) from dialkyl Zn and an oxygen source (water, peroxide, or alcohols) or spray pyrolysis have been published: from diethyl Zn [11], Zn acetate [12], Zn acetylacetonate [13], and Zn amides [14]. Also, theoretical studies using DFT (density functional theory) on ZnO obtained from diethyl Zn and water reaction has been published [15]. The hydrolysis reaction to produce $Zn(OH)_2$ is easy, but the formation of ZnO is very endothermic.

Dissociation of water on ideal surfaces of Zn (0001) has been controversial. Norton and co-workers reported dissociation on ideal surfaces [16], whereas Sen and Rao [17] reported that dissociation of water did not take place on this ideal surface. Dissociation of water induced by submonolayer coverage of atomic oxygen has been reported by Zhu and co-workers [18], Thomas and co-workers [19], and Norton and co-workers [16]. Other authors reported FTIR and XPS studies of water adsorbed onto clean Zn and ZnO surfaces, with evidence against and for dissociative or nondissociative adsorption of water [20–25]. There is evidence of nondissociative adsorption of water onto O-terminated ZnO and of dissociative adsorption of water on Zn-terminated ZnO. There is some experimental evidence for dissociative and nondissociative adsorption of CO on these surfaces of ZnO [26].

The objectives of this work are

(1) To analyze with a semiempirical method of the extended Hückel type (EHMO) the O_2 and H_2O adsorption on a bare Zn hexagonal metal surface (0001) and the first steps of ZnO formation, with up to four O_2 molecules taken up.
(2) Assuming the resulting surface from calculation, to study the O_2 and H_2O adsorption on the model of ZnO on Zn. The adsorption was studied using methods for sample/saturated solution preparation to set relative humidities (RH) published in Refs. [27] and [28].

Experimental results on the interaction between samples of metallic zinc and water vapor at different temperatures and RH, both in the absence and in the presence of oxygen, have been published by some of us in a previous manuscript. No theoretical or kinetic interpretation of the first steps of oxide formation was presented [29]. The products were identified as hydrated zinc oxides. In the runs conducted without oxygen the first portion of the kinetics for oxide formation and O_2/H_2O adsorption do not match. This fact implies that two processes are taking place: ZnO formation and reversible H_2O adsorption onto the oxide. When oxygen is present, no water adsorption takes place in the first hours, although oxygen and water participate in the ZnO formation with irreversible decomposition.

The results of this calculation are compared with the experimental results from Ref. [29] to present a picture of the damage at the metal surface, the initial step of growth of ZnO onto Zn, and the Zn/ZnO behavior in the presence of H_2O or H_2O/O_2 in the gas phase.

The nature of the reaction product was established by means of both ESCA–XPS (electron spectroscopy for chemical analysis–X-ray photoelectron spectroscopy) and GI-XRD (grazing incidence X-ray diffraction). The morphology of the surface was studied using SEM–EDAX (scanning electron microscopy–energy dispersive X-rays). These experimental facts are discussed with consideration of the modeling results, especially that the reaction involves the evolution of molecular hydrogen, as determined by gas chromatography. These data were not reported in Ref. [29], where only experimental adsorption data were presented.

2. Models and methodologies

2.1. Experimental

2.1.1. Description of the equipment and experimental procedure

A Cahn 1000 vacuum recording electrobalance in a thermostatically controlled room at 21 °C was used with continuous registration (registration speed: 2 cm/h and 10 mV = 1 mg). Saturated solutions (using high-purity salts) were used to obtain a known relative humidity (RH) following data published in Ref. [27]. The RHs were set at 0.3, 0.5, 0.60, and 0.94 and the temperatures at 21, 33, 42, and 50 °C. Once temperature and RH were fixed, blanks and samples were analyzed. The blanks were analyzed without a sample, with the registration of fluctuations due to buoyancy, especially at temperatures higher than room temperature. Samples were cleaned under vacuum of ca. 0.01 mmHg (1.33 Pa) using a mechanical pump. The blank and the sample took 24 h each to achieve constant weight. The tare was obtained in the absence of humidity. After this, the recipient with the

saturated solution was put in contact with the sample by opening a valve, and the variation of weight with time was registered until a constant weight was obtained.

To determine the amount of solid retained on the surface further evacuation was done after constant weight was reached. To desorb chemically bonded water, the temperature must be set to 200 °C in the case of ZnO [28].

When no O_2 is present, the balance was purged for 1 h using N_2 before measurements. The remaining oxygen was checked using a Varian 3700 with TCD and silica gel column and it was lower than 0.01% v/v. The same equipment was used when hydrogen evolution was analyzed. Without oxygen, hydrogen production from water decomposition achieves 0.05%, whereas with oxygen it is only 0.025%.

2.1.2. Preparation of bare Zn samples

Using 99.99% purity Zn (Carlo Erba) a procedure was performed to further purify the samples. Samples were fused in vacuum (0.01 mmHg) in a furnace at optimal conditions found after a careful test. Temperature was set to 430–440 °C for 15 h. The main objective is to segregate impurities and discontinuities in the metal. These imperfections must be eliminated before use. The samples were cooled slowly, following the reverse of the temperature–time sequence used for heating. Discs of width 0.9 mm and diameter 1 cm were cut from the samples. A mechanism for polishing was included, based on published reports using an aqueous solution of chromic oxide and sodium sulfate for chemical attack. The procedure of polishing includes several steps: cleaning with paper, chemical etching for 3.5 min, cleaning with leather cloth and high-purity alumina, Buehler grade 1 (5 μm), chemical etching for 1 min, cleaning with a billiards cloth and alumina grade 2 (1 μm), chemical etching for 30 s, cleaning with a leather cloth and alumina grade 3 (0.3 μm), and finally chemical etching for 10 s [27]. This procedure was able to produce reproducible samples. Sample discontinuities at the surface were avoided. This fact was checked using an optical microscope. It was observed that distortion is reduced after the first polishing with the leather cloth. The macrostructure of the surface is revealed after this.

2.1.3. The measurements of weight gain with and without O_2

Other details of the experimental data of thermogravimetric measurements can be found in Ref. [29]. The thermogravimetric measurements show for two different steps all RH conditions: a step of oxide formation on Zn (characterized by k_{ox}) and later a step of adsorption (characterized by k_{ads}). These steps are clearly shown in the kinetic curves for the thermogravimetric measurement [29].

2.1.4. SEM–EDAX

A JEOL 35CF, operated between 15 and 21 kV, with an EDAX of Si–Li was used (resolution 140 eV).

2.1.5. XPS

For the XPS measurements a Perkin–Elmer PHI 548 X-ray photoelectron spectrometer was used, with an Al anode and a concentric analyzer. The analyzer had a window of 50 eV, with a tension of 1500 V, a scan rate of 1.8 eV/s, a sensitivity of 3 K, and a range of scanning of 20 eV.

2.1.6. GI-XRD

The methods presented above were complemented with grazing incidence X-ray diffraction (GI-XRD), employing a PW 3710 diffractometer with a PW 1830 generator. Measurements were carried out using x-APD software linked to a file TADD (total access diffraction database).

2.2. The method

Details of the EHMO procedure can be found in Refs. [30,31]. The parameters used in the calculation (H_{ii} (eV), or ionization potential, and ξ_{i1}, or Slater exponents) were the following: for Zn4s, $\xi_{i1} = 2.01$, H_{ii} (eV) $= -12.41$; for Zn4p, $\xi_{i1} = 1.70$, H_{ii} (eV) $= -6.53$; for O2s, $\xi_{i1} = 2.1630$, H_{ii} (eV) $= -31.60$; for O2p, $\xi_{i1} = 12.7500$, H_{ii} (eV) $= -16.78$; for H1s, $\xi_{i1} = 1.0000$, H_{ii} (eV) $= -13.60$. The energies reported were calculated as the energy difference between the adsorbate at finite distances from the surface and the adsorbate and surface at infinite distance in the case of adsorption. When the reaction is analyzed, the energies are calculated considering the minimum found by calculation and an initial situation. The intention is not to model all the possible situations of ZnO growth and all the possible sites on the surface. Considering the experimental data and published reports about the most probable plane for ZnO growth, the theoretical calculation was performed on cluster/mechanisms for which experimental evidence exists, to support the proposals presented in Ref. [29] and here as speculation. The size of the cluster needed for this calculation makes the application of DFT (density functional theory) difficult because of the importance of relativistic problems in the convergence criteria.

2.3. The models

2.3.1. Zn surface

The Zn (0001) was modeled with an hcp structure. As reported by several authors [28,31–34], water interacts most strongly with the zinc sites available on the (001) and (100) faces and more weakly with the oxygen sites on the (001) and (100) faces, forming Zn oxyhydroxides. A few studies on the effect of crystallographic orientation on corrosion resistance of Zn have previously been reported [35,36]. In those studies single crystals or electrogalvanized coatings with well-defined surface orientation (0001), (1010), and (1120) were used. In these works, little effort has been devoted to investigating the influence of crystallographic orientation on passivity of Zn. From the results of Ref. [37], the oxide formation seems to be greater on grains of Zn

with a mainly exposed basal plane (0001). The grains have high packing density closer to that of the basal plane. Besides, this work showed a strong dependence of the cyclic voltagrams and capacities on the crystallographic grain orientation. Oxide formation was greater on low-index grains than on high-index ones. The growth is supposed to take place at the metal/film interface, thus inducing the strong dependence on the crystallographic surface structure of this interface. Some evidence of hexagonal cell structure in oxide films with a cell size of 3000 Å has been reported [38]. The excellent review of Henderson [38] was used to select the Zn surface and the main adsorption sites for O_2 and water on the surface of Zn (0001). Several theoretical studies on water dissociation have been published (see Section 1). Defects have long believed to be the most active sites for water dissociation. Two of the most studied oxide surface cases TiO_2 (110) and MgO (100) also represents the most controversial cases with regards to molecular vs dissociative desorption. The main point is how to achieve experimentally an ideal, well-characterized structure. The ambiguity regarding water dissociation on these surfaces posses a challenge to experimentalists and theorists [39]. The first step in the theoretical characterization is to simplify the problem: viz. an ideal structure and no interaction between adsorbates, in this case water and oxygen. We selected this approach for two reasons. First, the surface-defect concentration in Zn is difficult to characterize and to quantify (kind of site, environments, etc.). Moreover, there now exist many studies that propose water dissociation on zero-defect surfaces. Second, in the case of water–oxygen interaction, oxygen is said to catalyze water decomposition [39]; therefore we have the same products, but the reaction presents slightly different stoichiometry. Formation of ZnO by reaction of water with Zn is exothermic, with a reaction enthalpy of 120 kJ/mol. Trace levels of O_2 either dosed or as impurity catalyzes water dissociation. In the case of Zn (0001) there have been controversial results, being dissociation as a minor or major pathway or no dissociation detected. In the case of ZnO (0001), ZnO (000$\underline{1}$), ZnO (10$\underline{1}$0), or ZnO_2 (111), no dissociation of water is detected [6]. Some authors reported nondissociative adsorption of water on Zn (0001). Bulk phase thermodynamic properties cannot be used to predict surface processes on single crystal surfaces (see Ref. [39, p. 93]).

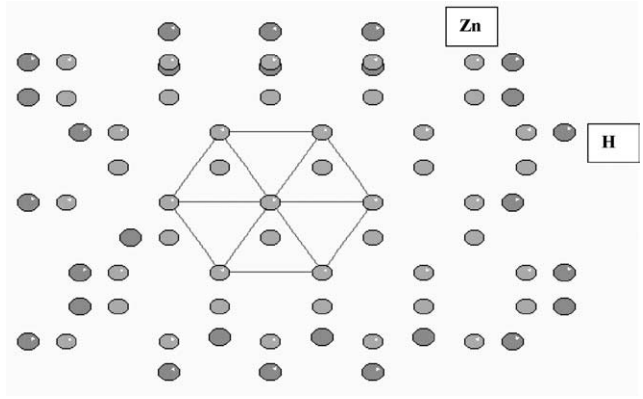

Fig. 1. Cluster for EHMO calculation.

Adsorption occurs preferentially at surface cation sites in metal and semiconductor surfaces, where the adsorbed species are stable even at room temperature [33]. The space group was $P63/mmc$ (space group 194) and the cell parameters selected were $a = b = 266.49$ pm, $c = 494.68$ pm, $\alpha = \beta = 90.0°$ and $\gamma = 120.0°$. A cluster with a total amount of 114 atoms for Zn plus border H (to prevent dangling bonds and border problems) was used: 46 H and 68 Zn atoms. Fig. 1 shows the complete cluster with three complete planes. O–O bond length in O_2 was set initially to 1.21 Å, whereas for the water molecule H–O was 0.96 Å.

Schemes 1 and 2 present a flow diagram of how the calculations presented in the following paragraphs were carried out for O_2/H_2O adsorption/dissociation on Zn and ZnO.

2.3.2. *Adsorption of water monomer and dimer on Zn*

The structure of surface-adsorbed water monomers and dimers was selected by considering reported data on the field [39]. Water was considered to adsorb in two ways: one water molecule per Zn atom or two water molecules per Zn

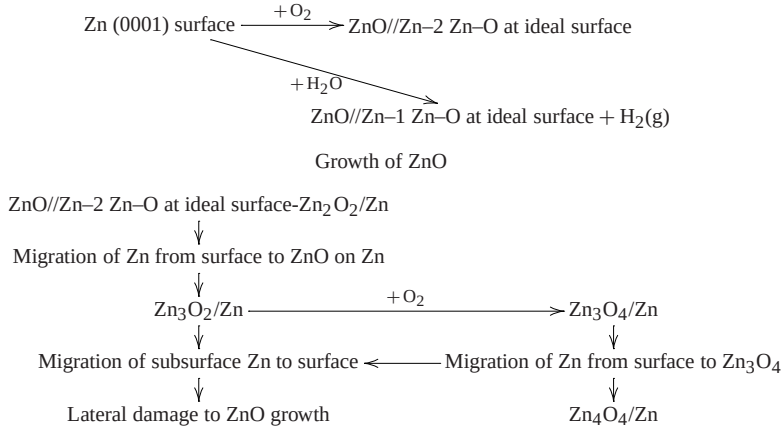

Scheme 1. Flow diagram of first O_2 adsorption on bare Zn and first steps of ZnO growth on Zn.

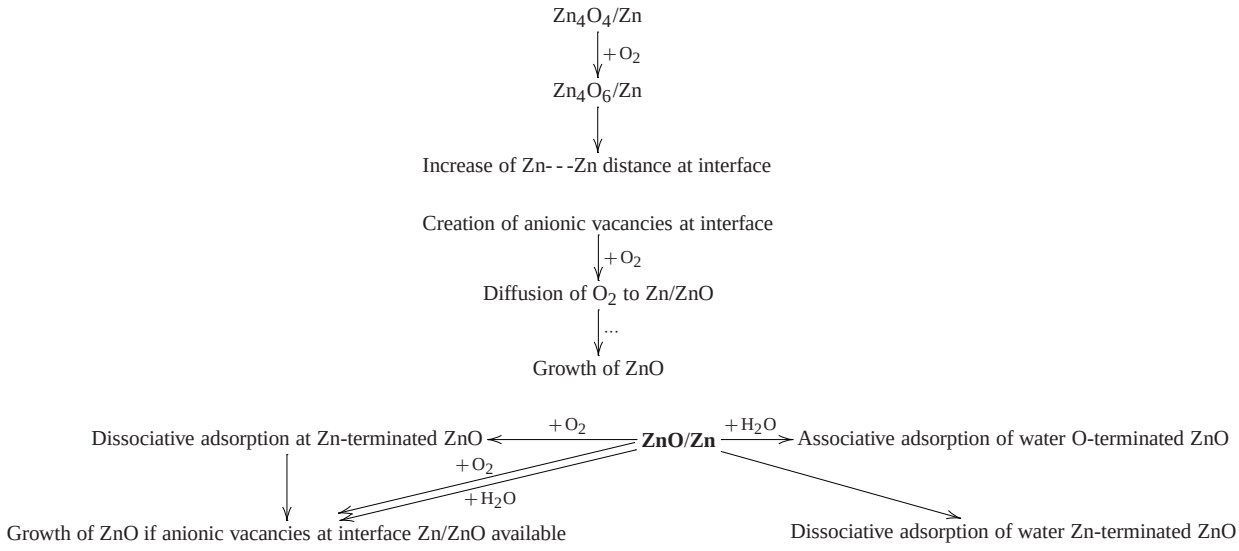

Scheme 2. Growth of ZnO on Zn—adsorption of O_2/H_2O onto ZnO.

atom, on top and in the middle of a complete hexagon. In the case of one H_2O, irreversible decomposition was modeled in three steps: adsorption of water, reaction to give H_2 with hydrogen from the same water molecule, and desorption of H_2. Finally, a Zn–O bond remains at the surface and a H_2 molecule is desorbed. This reaction produces a ZnO monolayer (see Fig. 2). When two H_2O are adsorbed onto the same Zn, the H_2 formation was modeled by reaction of hydrogen from different water molecules.

The final structure at the surface is $Zn(OH)_2$. It is important to address this reaction with a model of water dimer reaction on metal surfaces. Reaction of this structure to desorb water (reversible decomposition) was also modeled. In the case of the first layer of O, the final structure is Zn–O again (see Fig. 3).

2.3.3. *Adsorption of O_2 on Zn–ZnO formation*

The adsorption–reaction of O_2 was modeled, including O_2 adsorption on one on-top Zn atom and dissociation of O_2 by the increase of the O–O length. Twenty-eight steps were analyzed for the reaction of O_2 dissociation. The final structure is two near Zn–O bonds. In this sense, this reaction is very efficient, producing two Zn–O bonds in two steps. In this case ZnO was considered to have the wurtzite structure with $C_{4–6v}$ symmetry, with the oxygen atoms placed into the vertices of a slightly distorted tetrahedron (with nearest atomic distances Zn–O 1.992 and 1.973 Å). At the surface these distances are minor (see Fig. 2).

2.3.4. *Building of the ZnO structure*

Once two Zn–O bonds are present at the surface, a Zn vacancy is created on the ZnO monolayer. The occupancy of this vacancy was modeled in two ways:

(a) By diffusion of a surface Zn to the place between the oxygens of ZnO (see Figs. 4a and 4b).
(b) By interstitial diffusion of a subsurface Zn from the second layer (see Fig. 5).

Both movements lead to Zn occupying almost the same place on the oxide, but the defect location on the metal is different. In the case of (a), a metal vacancy is created at the surface. In the case of (b), a metal vacancy at the subsurface is created. The final structure is very oxygen deficient, because Zn is tetracoordinated to O in the most stable and common structure of ZnO. The Zn-terminated growing ZnO is oxygen-deficient.

After this, a second O_2 molecule was placed on the surface metal vacancy following route (a) of Zn migration. Zn subsurface diffusion to the oxygen atoms of this second dissociated molecule was considered. Finally, the structure of oxide is placed at longer Zn–Zn distances because of ZnO formation in the Zn–ZnO interface and these are sites for O_2 adsorption and reaction. In this case two more O_2 molecules were considered in the calculation.

In the case of interstitial Zn migration, a second O_2 molecule was adsorbed onto oxygen vacancies in the oxide. Zn subsurface migration to occupy the Zn vacancies in the Zn/ZnO interface was modeled. Migration of Zn at surface to occupy the Zn vacancies was also considered. In this sense, only reaction of O_2 with Zn-terminated oxide is important, and after occupancy of the anion vacancies on the Zn-terminated oxide, the O_2 dissociative adsorption on the oxide stops.

2.3.5. *ZnO surface*

The used ZnO surface was that resulting from the EHMO calculation. We performed oxygen and water adsorption

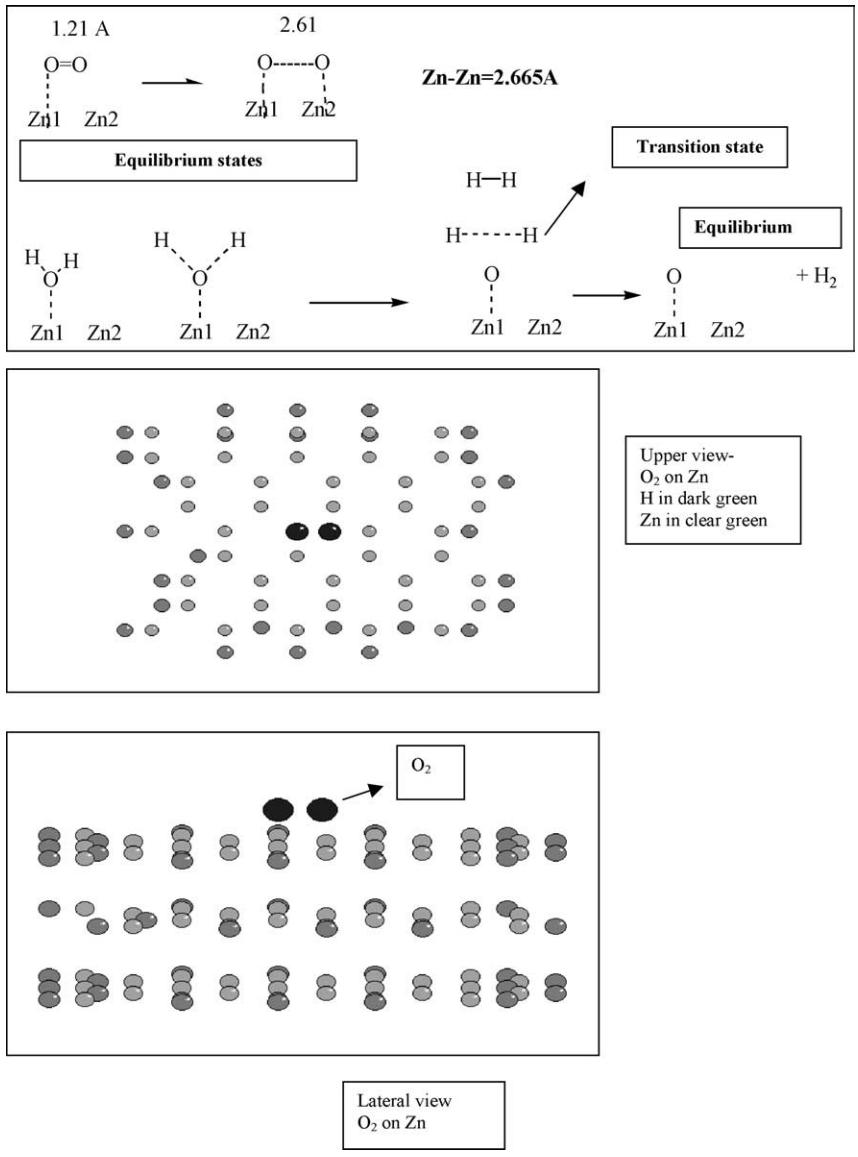

Fig. 2. Portion of cluster where O_2 and H_2O adsorption take place. Mechanism for O_2 adsorption and dissociation. Mechanism for one H_2O adsorption and dissociation.

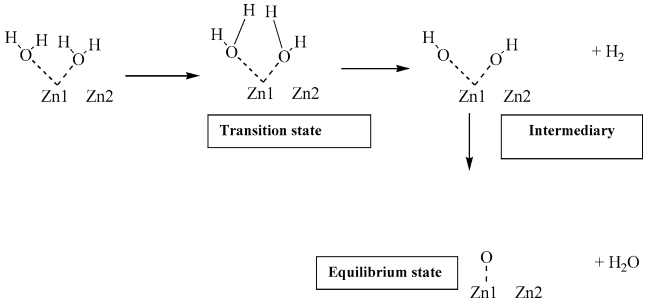

Fig. 3. Mechanism for two H_2O adsorption and dissociation on Zn–H_2 evolution.

on Zn from a local ZnO monolayer. This monolayer has strongly relaxed Zn–O bond (shorter than Zn–O bonds in ZnO bulk). Water adsorption was modeled because O_2 uptake is known to take place on anionic vacancies of the oxide. Reviews on oxide surfaces were also carefully analyzed to choose the selected theoretical study we used [39].

The growth of ZnO is possible if the interface Zn/ZnO has anionic vacancies available to incoming O_2 (see Scheme 2). The main point to consider here is the importance of Zn migration from the metal bulk to surface planes for the oxide formation. Moreover, it is not a trivial task to model the availability of oxygen adsorption sites at the interface Zn/ZnO. Under the initial conditions of surface attack, metal vacancies at the metal, which develop oxygen vacancies for the oxide in the interface, are the main sites for O_2/water adsorption. When the oxide grows the oxygen vacancies become less available and finally become inaccessible. Scheme 2 shows how the adsorption on ZnO was performed.

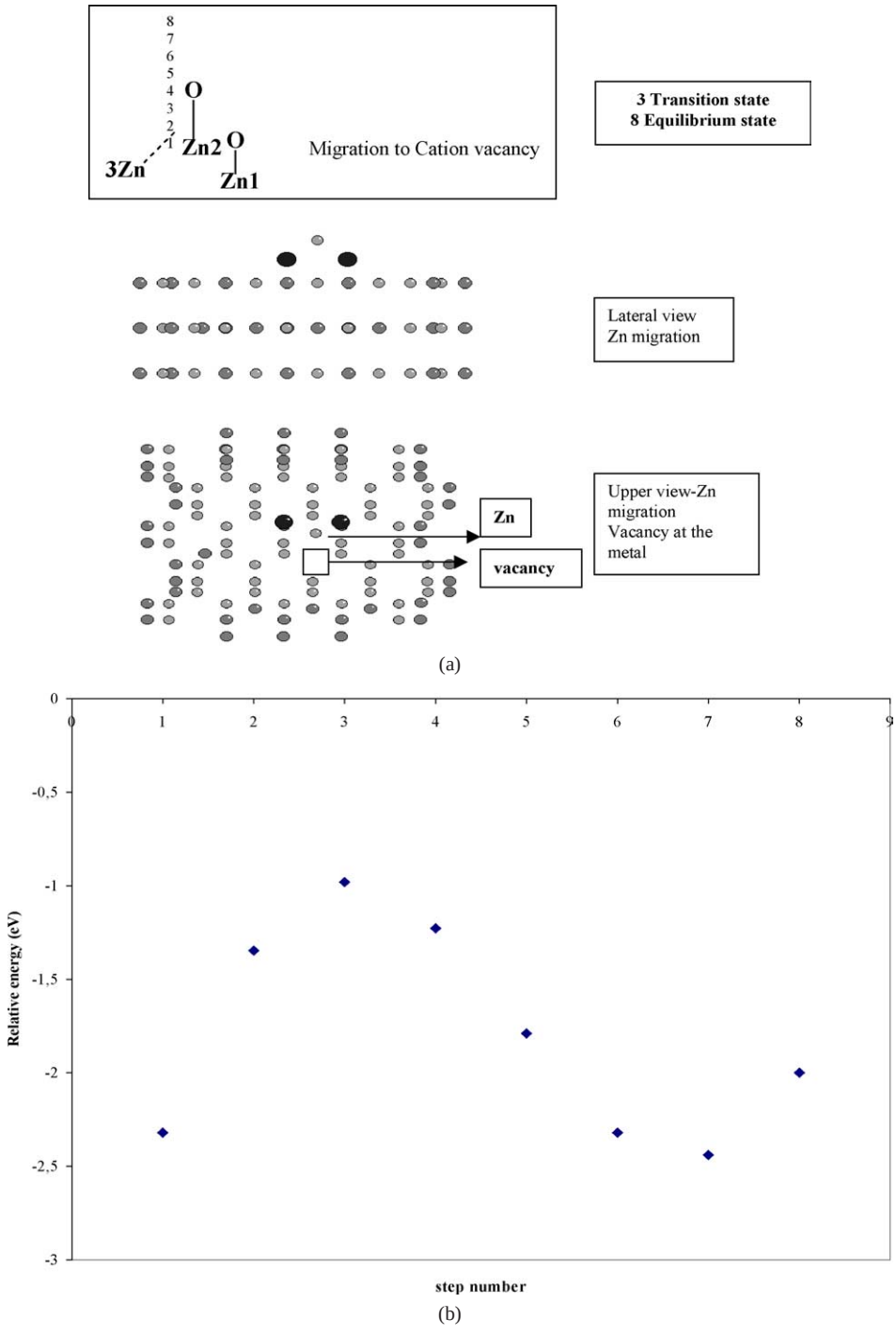

Fig. 4. (a) Migration of Zn through cation vacancies from metal to a cation vacancy in the oxide, steps 1 to 8. (b) Relative energy for steps 1–8 in Zn migration to a cation vacancy in ZnO.

3. Results of experimental characterization

3.1. Adsorption of O_2/H_2O

The quantity of adsorbed mass of O_2/H_2O was obtained by evacuation at each time (see Table 1). Remaining mass was considered the mass of oxide at each time.

Tables 2 and 3 present the kinetic analyses of all experiments with and without O_2.

Tables 4 and 5 present the adsorbed mass in the second step at different conditions of RH and temperature, with and without O_2.

3.2. XPS

The XPS spectroscopy determinations were also performed on samples reacted at high relative humidity (RH) and temperature. In this case, as Zn and ZnO have very

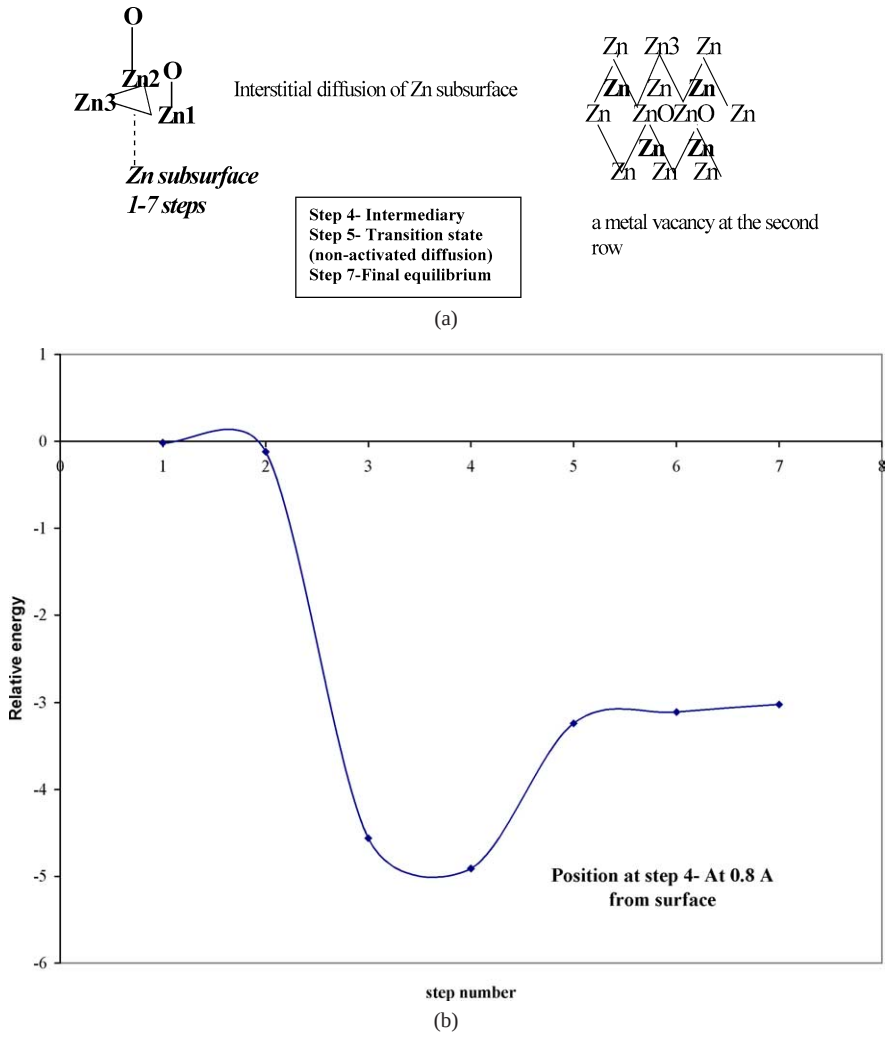

Fig. 5. (a) Interstitial diffusion of Zn subsurface in metal to a cation vacancy in the ZnO, steps 1 to 7. (b) Relative energy for steps 1–7 in Zn interstitial diffusion to a cation vacancy in ZnO.

Table 1
Experimental data: total mass gained at equilibrium in thermogravimetric experiments (in all cases $\times 10^7$ g/cm^2): E_a is activation energy

	21 °C	42 °C	50 °C
Without O_2			
E_a reaction = 34 kJ/mol, adsorption = 11 kJ/mol			
RH33			
M	56.4	211.6	–
M_{ox}	10.6	70.5	–
RH59			
M	–	700	1100
M_{ox}	–	254	536.1
With O_2			
E_a reaction = 21 kJ/mol			
RH33			
M	–	500	740
M_{ox}	–	150	300
RH94			
M	300	2400	1700
M_{ox}	100	1100	900

close binding energies that make their differentiation difficult, the O/Zn atomic ratio was calculated and found to have a value higher than one. ZnO and ZnO·2H_2O were used as standards. As this is generally ascribed to the presence of surface OH groups, it points to a residual layer of chemisorbed water. Thus, it is reasonable to conclude that the reaction product remaining after vacuum desorption is zinc oxide with some chemisorbed water, ZnO_nOH, as reported in the literature [1–3]. This can be seen from the data in Table 6.

3.3. SEM–EDAX

The surfaces were examined in a freshly state. The product formed varies depending on experiment conditions (RH, temperature, presence or absence of O_2) in terms of distribution, quantity, and severity of damage.

At high-humidity conditions, the increase of temperature increases the amount of product (see Figs. 6, 7, and 8). As well, there is a modification of the distribution of damage,

Table 2
Parameters obtained from gravimetric measurements under different conditions without O_2: k_{ad}, rate constant for adsorption; k_{ox}, rate constant for oxidation without O_2 (s^{-1})

HR	T [°C]	$k_{ad} \times 10^4$	$k_{ox} \times 10^4$	k_{ad}/k_{ox}	$k_{ox}/(HR)^n$	$k_{ad}/(HR)^{n'}$	$k^\circ_{ad}/k^\circ_{ox}$
0.94	21	3.1270	0.7485	4.18	0.81	3.58	4.42
0.90	33	3.6000	1.4980	2.40	1.72	4.54	2.64
0.88	42	4.3200	1.9412	2.23	2.29	5.10	2.23
0.85	50	4.9280	2.5896	1.90	3.20	6.09	1.90
0.59	21	1.2052	0.3867	3.12	0.77	3.85	5.01
0.52	42	2.6301	0.9466	2.78	2.21	6.15	2.78
0.50	50	2.8183	1.3000	2.17	3.20	6.94	2.17
0.33	21	0.3196	0.2039	1.57	0.86	3.66	4.25
0.33	33	0.4756	0.3214	1.48	1.36	5.45	4.01
0.32	42	1.1792	0.5050	2.34	2.22	5.19	2.34
0.32	50	1.3632	0.7189	2.78	3.16	6.00	1.90

n values between 1.3 and 1.4 obtained by correlation.

Table 3
Parameters obtained from gravimetric measurements under different conditions with O_2: k'_{ox}, rate constant for oxidation with O_2 (s^{-1})

RH	T [°C]	$k'_{ox} \times 10^4$
0.94	21	1.2589
0.88	42	2.2000
0.85	50	2.6000
0.59	21	0.8913
0.55	33	1.2162
0.52	42	1.4706
0.50	50	1.7000
0.33	21	0.5700
0.32	42	1.0000
0.32	50	1.1900

an effect whose causes can be attributed to RH and temperature. Under low-humidity conditions there is no high variation with the increase of the temperature and the attack is very disperse. Comparing the SEM images of products at equilibrium times (using high or low RH) at the same temperature the quantity of product increases with the increase of RH.

Considering Ref. [29], the samples were analyzed at initial and equilibrium times and also at different times of reaction. The analysis of the images in sequence permit us to conclude that initially the surface suffers a localized attack with the appearance of small and disperse particles (3–6 μm in diameter). The pit increases in width for high RH. Besides, the particles of product increase in size and quantity. At low RH the behavior is different (see Figs. 9 and 10).

The surface reaches equilibrium after 15–20 h exposure being the morphology close to that at 24 h. This fact agrees with the quantitative results from gravimetric measurements.

In all cases the EDAX analysis demonstrated that the composition is that of ZnO, with an O/Zn atomic percentage ratio of 1.11. SEM–EDAX shows that the lateral attack to the oxide is found at the Zn surface after experiments. In all cases, the observations revealed that the reaction does not form pits, but proceeds laterally. The product appears as small conglomerates whose size and distribution on the surface depend on the working conditions.

Table 4
Adsorbed mass in the second step with O_2: m, total adsorbed mass; m_{ox}, mass of hydrated oxide

RH	T [°C]	$m \times 10^5$ [g]	$m_{ox} \times 10^5$ [g]	$(m - m_{ox}) \times 10^5$ [g]	$(m - m_{ox})/m_{ox}$
0.33	21	2.0	0.38	1.62	4.30
0.33	33	4.0	1.29	2.71	2.10
0.32	42	7.0	2.35	4.65	1.90
0.32	50	10.5	4.20	6.30	1.50
0.59	21	3.6	1.60	2.00	1.30
0.55	33	8.6	4.10	4.50	1.10
0.52	42	17.8	9.50	8.30	0.87
0.50	50	28.5	15.90	12.60	0.79
0.68	21	4.7	2.48	2.20	0.89
0.61	42	24.0	14.00	10.0	0.71
0.94	21	8.3	2.83	5.47	1.93
0.90	33	28.0	13.80	14.20	1.03
0.88	42	32.6	16.10	16.50	1.02
0.85	50	51.0	28.65	22.35	0.78

Table 5
Adsorbed mass in the second step without O_2

RH	T [°C]	$m \times 10^5$ [g]	$m_{ox} \times 10^5$ [g]	$(m - m_{ox}) \times 10^5$ [g]	$(m - m_{ox})/m_{ox}$
0.33	21	0.8	0.15	0.65	4.30
0.33	33	1.7	0.44	1.26	2.80
0.32	42	3.3	1.00	2.00	2.30
0.32	50	6.5	2.00	4.50	2.20
0.59	21	1.8	0.63	1.20	1.85
0.52	42	9.5	3.80	5.70	1.50
0.50	50	16.0	7.60	8.40	0.90
0.94	21	4.1	1.20	2.90	2.40
0.90	33	8.0	3.00	5.00	1.60
0.88	42	15.0	7.60	7.40	0.97
0.85	50	24.0	13.80	10.20	0.74

Table 6
XPS data

	ZnO	$ZnO{\cdot}2H_2O$	Unknown this work
BE Zn (eV)	1021.6	1021.5	1021.3
BE O (eV)	531.6	531.6	531.6
O/Zn	1.40	3.5	1.45

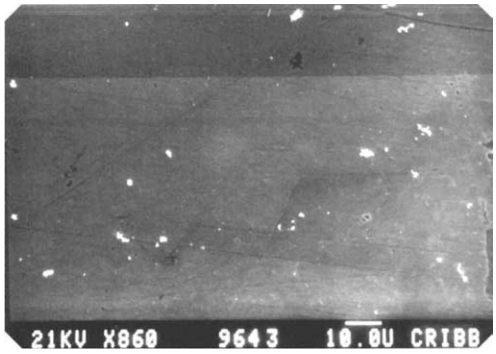

Fig. 6. Stabilized Zn surface at RH 0.94% and 21 °C.

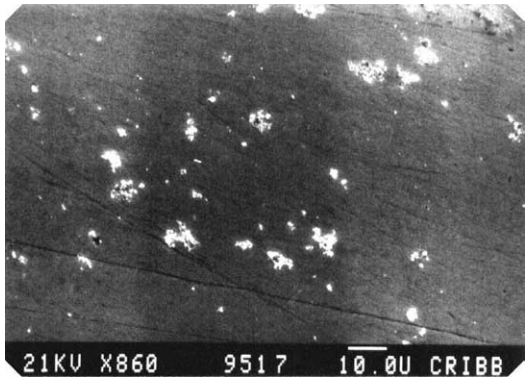

Fig. 7. Stabilized Zn surface at RH 0.94% and 40 °C.

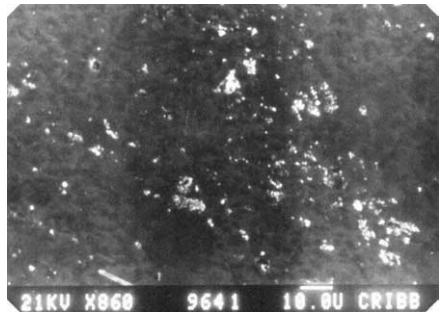

Fig. 8. Stabilized Zn surface at RH 0.94% and 60 °C.

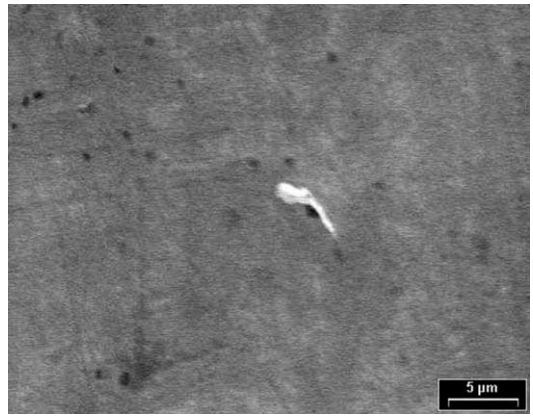

Fig. 9. Stabilized Zn surface at RH 0.33% and 21 °C—time of reaction 3600 s.

3.4. XRD

The diffractograms of the experiments here shown and Zn or ZnO standards were coincident. These phases were found as the only crystalline structures present (see Fig. 11). There are differences in the intensity of peaks at 35°, 48°, 63°, and 70° when the ZnO is obtained with or without O_2, but the profiles are very similar. It seems that when O_2 is absent, some planes of ZnO are better defined.

The crystallographic domains belonging to these planes have minor size when O_2 is present. This can be found from the broadening of the XRD peaks. Because of the nature of the reaction of Zn with O_2 (inactivated) and with H_2O (activated) it is clear that a more amorphous surface would be the result when O_2 is present.

Fig. 10. Stabilized Zn surface at RH 0.33% and 21 °C—time of reaction 9000 s.

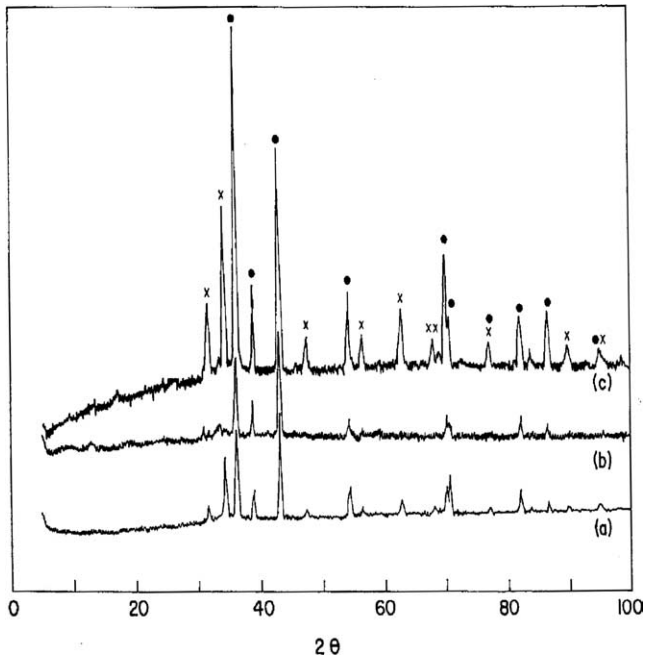

Fig. 11. X-ray diffractograms of the surface at equilibrium—HR 94% and 21 °C (a) in the presence of dry air, (b) in the presence of oxygen with water vapor, and (c) without oxygen with water vapor. Peaks correspond to (●) Zn, (×) ZnO.

4. Results of theoretical modeling

4.1. Adsorption of water on Zn

4.1.1. Monomer

Fig. 2 shows the steps of water adsorption–reaction. Twenty steps were analyzed for the total picture of the reaction. The energetic minima were found at −11.8 eV for monomer H_2O adsorption. The change in energy for the reaction of monomer H_2O adsorption is −7.5 eV. The H_2 desorption energy achieves +0.42 eV. All the steps of H_2 formation were considered, from the elongation of the O–H bond up to the decrease of the H–H bond (13 steps) with changes in 0.1 Å. The activation energy for H_2 formation found was near 0.3 eV or 30 kJ/mol.

4.1.2. Dimer

In this case two H_2O molecules were adsorbed onto Zn in 14 steps. Fig. 3 shows the whole reaction. The energetic minima were found at −12.1 eV for dimer H_2O adsorption. The change in energy for the reaction is −6.4 eV. In this case H_2 is lost easily, with −3.9 eV for the desorption reaction. The formation and release of water to leave a Zn–O bond at the surface involves a change of −0.9 eV in a nonredox reaction. The release of H_2 to leave two Zn–O bonds, in contrast, is strongly favored (−20 eV). This is a redox reaction.

4.2. Adsorption of O_2 on Zn

The adsorption–reaction of O_2 onto Zn is not an activated process. The energetic minimum is found at −36.3 eV when assuming the O_2 and Zn at infinite distance from each other as the initial situation and two Zn–O bonds of length near 1 Å at the surface as the final situation.

4.3. Building of the ZnO structure

4.3.1. Initial cation diffusion by vacancies

The energy found for the whole reaction of initial diffusion of a surface Zn to a position between the oxygens of ZnO were −2.44 eV with an activation energy of +144 kJ/mol (see Fig. 12). The second O_2 molecule adsorption was considered in the x-axis or the y-axis and the y-axis was preferred (−10.8 vs −3.3 eV). Dissociation of this second O_2 molecule was analyzed in eight steps to be both O's finally placed on surface Zn. The change in energy was −20.7 eV. The migration of subsurface Zn to the surface was studied (from −2.43 Å to 0 in z). This nonactivated process involves a change in energy of −2.9 eV. The migration of another subsurface Zn to occupy this vacancy was an inactivated process with almost no change in total energy (+0.1 eV). In this case the migration of the cation vacancy is considered. The additional migration of a surface Zn to occupy the place of the second Zn was analyzed in 14 steps. In this case the Zn diffusion from the surface to occupy the vacancies at the subsurface has an activation energy of 1.03 eV (see Fig. 12).

4.3.2. Cation interstitial diffusion

The energies found for the whole reaction of interstitial diffusion of subsurface Zn from the second layer was −4.9 eV and nonactivated (see Fig. 5). After this a second O_2 molecule was placed on Zn terminated oxide at the same distance that these obtained in the first O_2 adsorption, with a change in energy of −32 eV. The increase in z (+0.2 Å) for the oxide produces an increase in energy (+0.8 eV). It seems that the increase in energy for this process can be compensated for by the decrease in energy when O_2 is adsorbed and

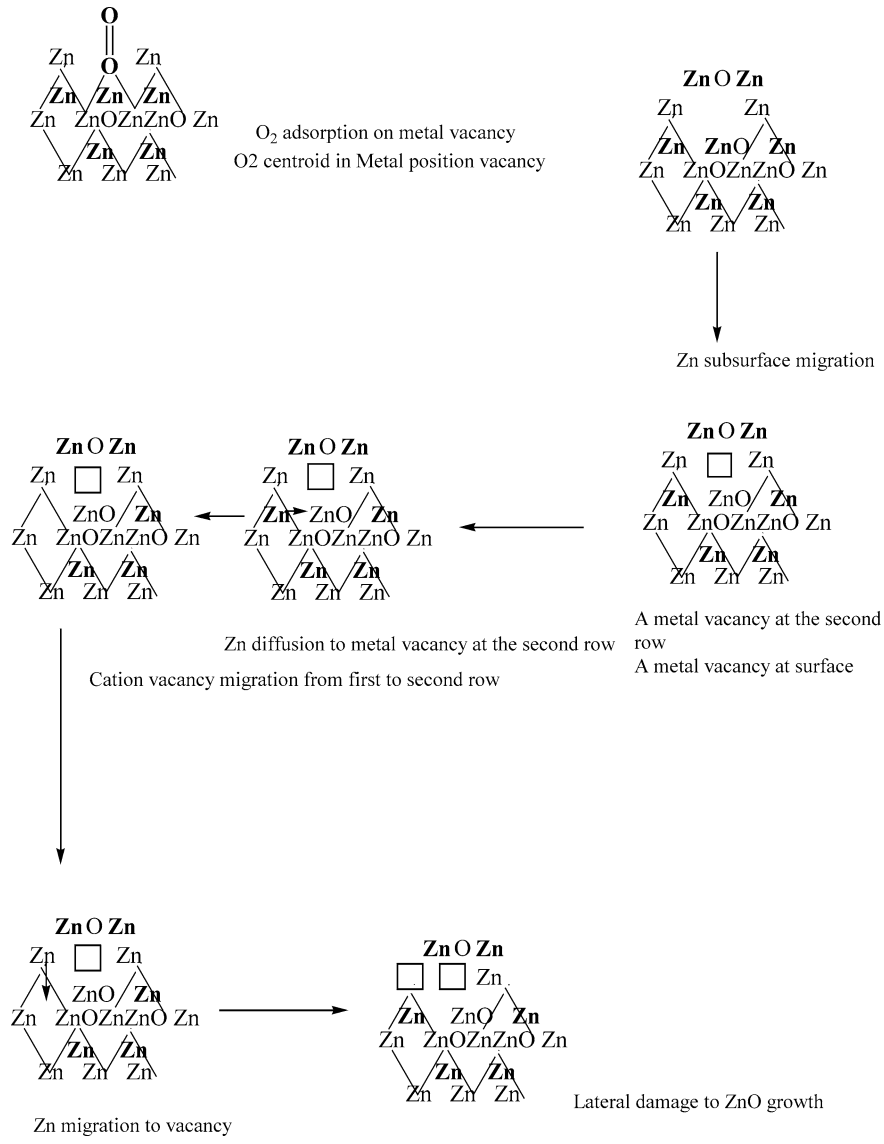

Fig. 12. Steps of ZnO growth. O_2 adsorption on a metal vacancy in the interface, migration of Zn subsurface to surface, migration of Zn subsurface to vacancy subsurface, migration of Zn at surface to subsurface: lateral damage.

reacted on metal vacancies that develops oxygen vacancies at the interface. When the surface Zn migrates to occupy the vacancy of the subsurface Zn, there is a free space for further O_2 adsorption. The adsorption of O_2 and migration of one O to inside the metal (-0.2 Å in z) is favored by -30.6 eV. O_2 was considered to migrate in the metal when metal vacancies at the first and second row are found (see Fig. 13).

4.4. Adsorption of water on ZnO model

Considering the whole structure, adsorption of water was analyzed in two ways: parallel or perpendicular to the surface. The better geometry was perpendicular. In both cases, adsorption energies are low (-0.58 and -0.73 eV) (see Fig. 13).

Using a simpler model from the first O_2 reaction, reaction of dissociation of H_2O was considered to produce OH at the oxide surface with -1.1 eV as the energy change. But from these results, it is clear that total dissociation is not favored with an increase of $+2.4$ eV for dissociation. The best final situation is hydrogen onto O from the Zn–O and the remaining OH between 2 Zn. Dissociation of OH is not favored. It seems that, more than dissociation, associative adsorption is favored. When the final structure is that depicted in Fig. 14, the change in total energy is -1.31 eV to achieve (c). The geometry depicted in Figs. 14a–14d involves a change of $+2.4$ eV.

In the case of migration of Zn for ZnO growth, the EHMO calculation gave evidence that Zn interstitial diffusion is the preferred way, as Macdonald and co-workers proved for electrochemical conditions in solution [6–9].

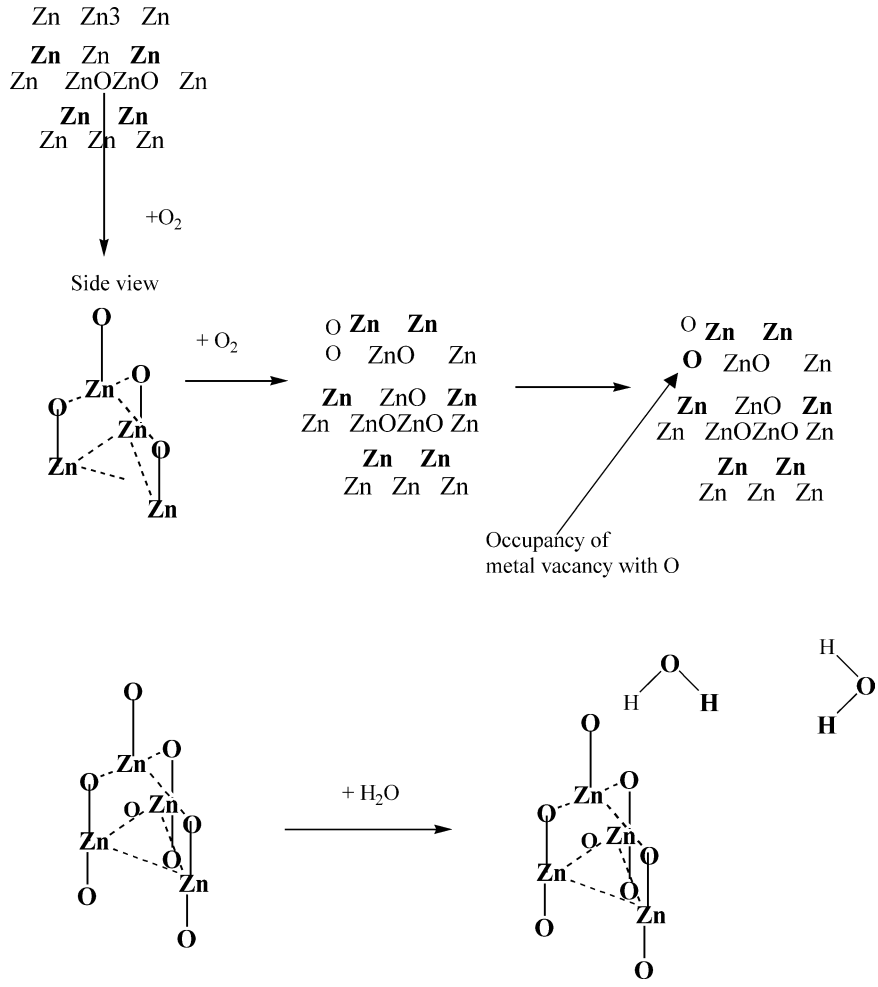

Fig. 13. Growth of ZnO by vacancy occupancy at interface with O_2/H_2O from gas phase: adsorption of water on ZnO.

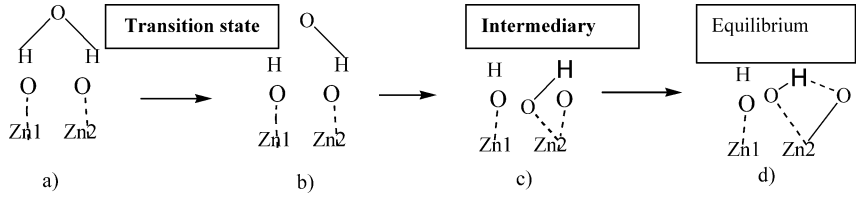

Fig. 14. Dissociation of water at ZnO surface.

5. Discussion and conclusions

5.1. Theoretical findings

When O_2 is not present, the oxide at the surface is provided by irreversible decomposition of water and H_2 evolution. This step is activated with an activation energy of 0.30 eV when water monomer is considered, obtained by EHMO calculation. It seems that the strong exothermic adsorption and reaction of water on the surface compensate for the activation energies for Zn interstitial migration. The activation energy for H_2 evolution is the same as the whole reaction activation energy. Dissociation of water at the surface seems to be the rate-limiting step. The water adsorption/reaction catalyzes Zn interstitial migration and EHMO calculations show this fact.

When O_2 is present, the oxide at the surface is provided by irreversible decomposition of water, H_2 evolution, and irreversible O_2 decomposition. This last step is almost non-activated. It seems that the strong exothermic adsorption and reaction of oxygen/water on surface compensates the activation energies for Zn interstitial migration. In other words, the O_2/water adsorption catalyzes the Zn migration. The activation energy for H_2 evolution from water, in this case catalyzed by O at surface and therefore lower than in the other case, is that of the global reaction experimentally found. The final picture is this: once the ZnO is formed (by O_2 dissociation or water decomposition with H_2 evolution), the H_2O is

adsorbed reversibly, without H_2 evolution on the oxide. Zn (0001) has been reported to produce H_2 without the H_2O–O intermediate, whereas Au (111), Ni (001), and Ru (0001) form this intermediate [39]. This mechanistic fact seems to be related to the thermodynamics at surface. Dissociation of H_2O takes place on anionic vacancies in Zn-terminated ZnO, leading to ZnOHOHZnO species at the ZnO surface, as demonstrated (see Figs. 14a–14d) by EHMO calculations.

5.2. Experimental evidence from our own lab work

The experimental activation energy for ZnO formation without O_2 is near 30 kJ/mol (see Table 1). Looking at Table 2, is clear that k_{ox} and k_{ads} increase with temperature and k_{ads}/k_{ox} decrease with the increase of temperature. As Table 1 shows the oxide formation becomes relatively more favored with increasing temperature. Hence, both groups of results agree with the idea that a higher amount of oxide forms at the surface with increasing temperature. Experimental data from kinetic measurements and SEM micrographs have shown this without doubt. XPS and XRD measurements demonstrated that dissociation of H_2O takes place on anionic vacancies in Zn-terminated ZnO, leading to ZnOHOHZnO species at ZnO surface. In case of ZnO or unknown samples, the O/Zn molar ratio is not 1 but 1.45, because at the surface a composition as presented above is expected (ZnOH OHZnO or 3O/2Zn = 1.5O/Zn). On O-terminated surfaces, water is adsorbed reversibly and no dissociation takes place. This picture arises whatever the condition of contact procedure. When O_2 is not present, the reaction is slower and the reaction rate increases with temperature at the same RH. The mass of oxide formed is doubled (with or without O_2) comparing 42 and 50 °C and 59 or 33% RH. Table 3 shows the k_{ox} obtained through a linear regression. It is clear that higher temperature increases k_{ox}. Therefore we expect more oxide formed at higher temperatures. The fact that at RH of 94% and 50 °C the increase in mass is lower than at 42 °C can be related to the exothermic character of the adsorption–reaction of water. When the RH is lower, the reactions of decomposition and H_2 evolution predominate on adsorption but at high RH the strongly exothermic adsorption predominates. In this case, the different shape of adsorption curves can be found: linear in the case of fixing at 42 °C the temperature between 10,000 and 50,000 s (time of reaction), and S-shaped in the case of 50 °C between 10,000 and 60,000 s (time of reaction) (see Figs. 3 and 5 or Ref. [29]).

5.3. General discussion of theoretical and experimental data

Several facts must be considered taking into account the results of EHMO calculation: Interstitial Zn diffusion is the favored process for ZnO formation. The key is the metal vacancies generation at the interface. These sites are the points for O_2/water adsorption and ZnO growth. If the thickness of ZnO barrier impedes the effective O_2 diffusion to achieve the vacancies at the interface, the ZnO formation is stopped. This fact is supported by our previous work, reported in [29]. After a period of growth, the oxide formation at the surface stopped. A barrier layer thickness and anionic vacancies elimination dependence of O_2/water diffusivity must be taken into account. This fact has not been considered in the published Macdonald papers because no O_2/H_2O–metal gas phase reaction was analyzed [6–9]. The proposal of the present work is the following. Adsorption of water onto bare Zn from the gas phase is from an activated process. This fact has been proved experimentally (see Table 1) and theoretically (see results section for the theoretical calculation). On-top adsorption of water in metal surfaces has been reported for Ru (0001). These kinds of sites are the most acidic and they favor electron transfer from O to metal. The prevailing long-range structure of adsorbates on cp structures is the $(\sqrt{3}\times\sqrt{3})$R30 structure. Other adsorbate distributions include $c(2\times 2)$. The adsorption takes place at the O side of water in the case of the metal surfaces and no changes in bond length take place at this first step. The angle is slightly reduced upon adsorption but no conclusive experimental data are available because in the case of LEED or photoelectron diffraction scattering, cross sections for hydrogen are extremely small [39].

When oxygen is present, oxygen competes with water for the same sites. In the case of water, hydrogen evolution takes place because of dissociative adsorption of water on Zn, again proven theoretical and experimentally. The Zn migration of subsurface/surface Zn to subsurface vacancies produced by interstitial migration to metal vacancies in the Zn/ZnO interface generates lateral damage to the growing oxide that can be seen by SEM–EDAX–XPS studies. This is the mechanism for the ZnO growth and lateral damage (through pit formation near ZnO) that constitutes the hypothesis of this study. The kinetic data can be explained using this surface model. O_2 or water dissociation at the bare Zn surface produces the same Zn–O bonds, a fact we could prove by EHMO calculation, and it was demonstrated by surface analysis of the ZnO samples obtained at different experimental conditions. H_2O coordinates reversibly to the nondefective oxide on O-terminated ZnO or dissociatively on anionic vacancies on Zn-terminated ZnO. Anionic vacancies in the growing oxide are the sites for O_2/H_2O adsorption. When O_2 is present, both compete for the sites and therefore a lower number of sites is available to H_2O (see Tables 4 and 5). The parameter defined as $(m - m_{ox})/m_{ox}$ is the total mass (m) minus the mass of oxide (m_{ox}) divided the mass of oxide. Experimentally, when O_2 is present, the m_{ox} and $m - m_{ox}$ parameters are higher and the $(m - m_{ox})/m_{ox}$ is lower than without O_2. Without O_2, the absolute amount of adsorbed mass is lower. The mass of adsorbed substrates relative to oxide mass is lower with O_2. Changes in kinetic curves with time arise because, first, we are obtaining data of oxygen and/or water adsorption/dissociation on bare Zn, and afterward of oxygen and/or water adsorption/dissociation on ZnO.

Acknowledgments

The authors want to acknowledge financial support from UNS. M.L. Ferreira acknowledges financial support from CONICET. J.C. Bazán acknowledges financial support from CIC.

References

[1] T.E. Graedel, J. Electrochem. Soc. C 193 (1989) 136.
[2] J.P. LaFemina, Surf. Sci. Rep. 16 (1992) 133.
[3] J.E. Jaffe, N.M. Harrison, C.A. Hess, Phys. Rev. B 49 (1994) 11153.
[4] C.B. Duke, R.J. Meyer, A. Paton, P. Mark, Phys. Rev. B 18 (1978) 4225.
[5] H. Overbury, Surf. Sci. 410 (1998) 106.
[6] D. Macdonald, Pure Appl. Chem. 71 (6) (1998) 951.
[7] D.D. Macdonald, S.R. Biaggio, H. Song, J. Electrochem. Soc. 170 (1992) 139.
[8] K. Ismail, D.D. Macdonald, E. Sikora, J. Electrochem. Soc. 145 (1998) 3141.
[9] D.D. Macdonald, J. Electrochem. Soc. 139 (1992) 3434.
[10] T. Barr, J. Vac. Sci. Technol. 14 (1) (1977) 660.
[11] J.H. Hu, R.G. Gordon, J. Appl. Phys. 71 (1992) 880.
[12] T. Maruyama, J. Shionoya, J. Mater. Sci. Lett. 11 (1992) 170.
[13] T. Minami, H. Sonohara, S. Takata, H. Sato, Jpn. J. Appl. Phys. 33 (1994) 1743.
[14] S. Suh, L.A. Milnea, D.M. Hoffman, Z. Zhang, W.K. Chu, J. Mater. Sci. Lett. 20 (2000) 115.
[15] S.M. Smith, B. Schlegel, Chem. Mater. 15 (2003) 162.
[16] B. Li, K. Griffiths, C.S. Zhang, P.R. Norton, Surf. Sci. 370 (1997) 7.
[17] P. Sen, C.R. Rao, Surf. Sci. 172 (1986) 26.
[18] C.T. Au, M.W. Roberts, A.R. Zhu, Surf. Sci. 115 (1982) L117.
[19] A. Farley, P.R. Davies, M.W. Roberts, N. Shukla, Y. Song, K.K. Thomas, Appl. Surf. Sci. 81 (1994) 265.
[20] G. Zwicker, K. Jacobi, Surf. Sci. 131 (1983) 179.
[21] V. Maurice, K. Takeuchi, M. Salmeron, G.A. Somorjai, Surf. Sci. 250 (1991) 99.
[22] K. Takeuchi, S.S. Perry, M. Salmeron, G.A. Somorjai, Surf. Sci. 323 (1995) 30.
[23] J.R. Creighton, J.M. White, Chem. Phys. Lett. 92 (1982) 435.
[24] Y.C. Kang, M.M. Milovancev, D.A. Claus, M.A. Lange, R.D. Ramsur, J. Nucl. Mater. 281 (2000) 57.
[25] C.T. Au, M.W. Roberts, Proc. R. Soc. London Ser. A 396 (1984) 165.
[26] Th. Becker, M. Kunat, Ch. Boas, U. Burghaus, Ch. Wöll, J. Chem. Phys. 113 (15) (2000) 6334.
[27] A. Tegart, The Electrolytical Chemical Polishing of Metals, second ed., Pergamon, 1959.
[28] T. Morimoto, M. Nagao, Bull. Chem. Soc. Jpn. 43 (1970) 3746.
[29] G.A. Alimenti, M.E. Gschaider, J.C. Bazán, J. Therm. Anal. Calor. 55 (1999) 569.
[30] G. Calzaferri, L. Forss, I. Kamber, J. Phys. Chem. 93 (1989) 5366.
[31] A.B. Anderson, J. Mol. Catal. 54 (1989) 281.
[32] M. Nagao, J. Phys. Chem. 75 (1971) 3822.
[33] P. Thiel, T. Madey, Surf. Sci. Rep. 7 (6) (1987) 211.
[34] R.F. Ashton, M.T. Hepworth, Corrosion 24 (1968) 50.
[35] H. Park, J.A. Spuznar, Corrosion Sci. 40 (1998) 525.
[36] C.J. Park, M.M. Lohrengel, T. Hamelmann, M. Pilaski, H.S. Kwon, Electrochim. Acta 47 (2002) 3395.
[37] H. Fry, M. Whitaker, J. Electrochem. Soc. 106 (1959) 606.
[38] M.A. Henderson, Surf. Sci. Rep. 46 (2002) 1.
[39] B. Li, K. Griffiths, C.S. Zhang, P.R. Norton, Surf. Sci. 370 (1997) 97.